Robotics and Computer-Integrated Manufacturing 37 (2016) 57–67

Contents lists available at ScienceDirect

Robotics and Computer-Integrated Manufacturing

journal homepage: www.elsevier.com/locate/rcim

Effect of technical parameters on porous structure and strength of 3D printed calcium sulfate prototypes

Mitra Asadi-Eydivand [a,*], Mehran Solati-Hashjin [a,b], Arghavan Farzad [a], Noor Azuan Abu Osman [a]

[a] Department of Biomedical Engineering, Faculty of Engineering, University of Malaya, 50603 Kuala Lumpur, Malaysia
[b] Biomaterials Center of Excellence, Amirkabir University of Technology, 15914 Tehran, Iran[1]

ARTICLE INFO

Article history:
Received 16 January 2015
Received in revised form
18 June 2015
Accepted 25 June 2015
Available online 8 July 2015

Keywords:
Process optimization
3D printing
Mechanical properties
Bone tissue Engineering
Dimensional accuracy
Rapid prototyping

ABSTRACT

Additive manufacturing methods such as three-dimensional printing (3DP) show a great potential for production of porous structure with complex internal and external structures for bone tissue engineering applications. To optimize the 3DP manufacturing process and to produce 3D printed parts with the requisite architecture and strength, there was a need to fine-tune the printing parameters. The purpose of this study was to develop optimal processing parameters based on a design of the experiments approach to evaluate the ability of 3DP for making calcium sulfate-based scaffold prototypes. The major printing parameters examined in this study were layer thickness, delay time of spreading the next layer, and build orientation of the specimens. Scaffold dimensional accuracy, porosity, and mechanical stiffness were systematically investigated using a design of experiment approach. Resulting macro-porous structures were also studied to evaluate the potential of 3DP technology for meeting the small-scale geometric requirements of bone scaffolds. Signal-to-noise ratio and analysis of variance (ANOVA) were employed to identify the important factors that influence optimal 3D printed part characteristics. The results showed that samples built using the minimum layer thickness (89 μm) and *x*-direction of build bed with 300 ms delay time between spreading each layer yielded the highest quality scaffold prototypes; thus, these parameters are suggested for fabrication of an engineered bone tissue scaffold. Furthermore, this study identified orientation and new layer spreading delay time as the most important factors influencing the dimensional accuracy, compressive strength, and porosity of the samples.

1. Introduction

Scaffolds play an important role in tissue engineering solutions to bone healing. Bone itself is known for its self-healing ability. However, a typical bone remodeling processes may not repair large-scale bone defects, and addressing significant bone losses remains a major challenge. Bone tissue engineering (BTE) is a potential solution to this problem as it integrates the use of cells and engineered materials to restore bone tissue. BTE scaffolds must possess myriad properties to meet application requirements [1]. Essentially, BTE scaffolds must provide a host-tissue-like mechanical support to promote neo-tissue growth and function. In fact, an ideal scaffold should resemble the natural extracellular matrix (ECM) of the cells. Scaffolds can be made from either natural or synthetic materials capable of forming a helpful micro-environment that allows proper generation of neo-tissue to repair and replace damaged or weakened organs and tissues [2]. Such scaffolds should provide sufficient porosity and permeability for nutrient transfer and removal of metabolic wastes [3]. In addition, for the reconstruction of complex bone defects such as osteoporotic fractures, we need patient-specific BTE implants with proper internal structure and mechanical properties. Appropriate materials and processing techniques should be employed to make implants and scaffolds with the requisite properties.

Rapid prototyping (RP) techniques which are promising potential fabrication methods for BTE scaffolds. RP techniques,, can fabricate a complex internal and external structure based on computer tomography (CT) data or prefabricated structure design such that it is possible to fabricate scaffolds with predetermined properties [4,5].

The high reproducibility of RP is an added benefit for clinical applications [6]. RP techniques typically begin with a CT scan of the defect site that gives the necessary data for making an accurate and precise three-dimensional (3D) shape of the defect. This pattern then is used as a guide to fabricate the 3D object [7]. One

Text for Footnote 1

* Corresponding author.
E-mail address: mitra@um.edu.my (M. Asadi-Eydivand).

http://dx.doi.org/10.1016/j.rcim.2015.06.005

particular method, namely 3D powder printing is a technology developed in the early 1990s at MIT (Cambridge, MA) [8]. It is based on the binding of powder particles by injecting a reactive solution in a layer-by-layer process until the structure is complete.

In recent years, there have been many reports on 3DP fabrication of BTE scaffolds and on critical process factors and parameters [9]. Various parameters affect the dimensional accuracy and mechanical properties of 3D printed specimens, which are the most important factors for evaluation fabrication parts. These parameters can be categorized into three main groups: (1) the machine setting parameters, (2) the chemical and physical properties of the powder and the binder, and (3) the structural design of the scaffolds. Many studies focused on improving the dimensional accuracy and mechanical properties of 3D printed objects have shown sensitivity to process parameters that can be tuned to improve the desired attributes. Patirupanusara et al. [10] looked at the effect of different compositions on physical and mechanical properties of fabricated 3D printed samples. Castilho et al. [11] fabricated cylindrical scaffolds with biocompatible and biodegradable materials and evaluated them in terms of geometric accuracy and the uniaxial compression behavior on the process directionality. Another study [12] focused on the synthesis and characterization of a novel powder system for a 3DP process. Butscher et al. [13] evaluated the 3DP process in terms of powder physical properties and reported the relation between powder properties including flowability and wettability with the final 3D printed scaffold properties. Many recent studies regarding the complexity of 3DP processes, have focused on proper printer setting parameters. In another study, Butscher et al. [14] systematically analyzed the relationship between layer thickness and layer stability with the quality of the final printed specimens. Alternatively, Suwanprateeb et al. [15] prepared adhesive pre-coated hydroxyapatite powders using hot plate drying coupled with a grinding technique with the aim of increasing the mechanical properties of 3D printed samples.

Several other studies have also focused on process parameter optimization while using commercially available materials. Hsu and Lai [16] studied the Taguchi experimental design method for optimizing part dimensional accuracy, reducing fabrication time, and reducing binder consumption *via* control of four factors: layer thickness, binder saturation values shell and core, the location of green-parts, and powder type of the specimens printed by ZCorp Z402 3DP. Although they managed to achieve their stated goals, the specimens were not optimized for the specific application. Suwanprateeb et al. [17] conducted a study focused on an investigation into printer parameters including layer thickness and saturation ratio and their effects on microstructure and mechanical properties using ZCorp Z400. Castilho et al. studied the potential of 3DP technology to fabricate scaffold prototypes for tissue engineering in terms of geometry. The smallest size for a well-defined pore they could achieve was 1 mm for a cubic unit cell with a side length of 10 mm [18].

The design, geometry optimization, and mechanical assessment of porous scaffolds still need further development. This is necessary for successful use of the scaffolds in bone tissue engineering. Furthermore, while the behavior of scaffold geometries can be accurately simulated with finite element modeling (FEM), predicting real strength and stiffness values depends on dimensional accuracy. Although several experiments have been conducted using 3DP technology to make scaffolds, there is still a need for further development focused on identifying mechanical and biological properties that are suitable for bone regeneration. Additionally, the limits and difficulties described in the literature also provided motivation for developing improved fabrication methods that would allow the user some control over the scaffold internal structure. One way to achieve these goals, without major changes to the already developed hardware and software architecture, is to re-tune and fine-tune the control factors of the existing rapid prototyping process for a given machine.

Powder and binder selection is an example of a factor that is not a process parameter but is important in determining part structure and quality. However, without comprehensive knowledge of design and process parameters, the resultant 3D printed parts may not have the desired properties or internal structure despite using the proper materials. The purpose of this study was to develop optimal processing parameters based on a design of experiments approach and to evaluate the 3DP process potential using optimized parameters for porous prototype fabrication.

In the present work, we have reported the fabrication and characterization of cylindrical calcium sulfate-based scaffold prototypes. We have used a design of experiments approach to optimize the design and fabrication process using a powder-based 3D printer (Zprinter® 450, Z-Corporation, Burlington, USA). The major printing parameters explored in this study are layer thickness, delay time of spreading the new layer, and build orientation of the specimens. Scaffold dimensional accuracy, porosity, and mechanical stiffness have been comprehensively studied by a design of experiment investigation. Resulting macro-porous structures have been analyzed and also evaluated in terms of technological potential for meeting the small-scale geometric requirements of bone scaffolds. The results of this study can be used as a guideline for adjusting the printing parameters for a particular application and material combination selection. Through the process-property optimization, improved 3D scaffolds can be printed using the same or different materials and/or other post-processing techniques.

2. Materials and method

We used a 3D-printing machine Zprinter® 450 (Z-Corporation, Burlington, USA), to produce cylindrical scaffolds (6 mm in diameter and 12 mm in height) prototypes. All the materials used, a high performance composite material (Zp150) and a water-based binder (Zb63), were also supplied by Z Corporation. After printing, all the specimens were held in the machine and dried for 90 min at ambient temperature. Then the printed porous bodies were depowdered by compressed air to remove any trapped and unbound powder. In this study, we avoided any further post hardened or infiltrate to eliminate parameters other than the design of experiments factors which may affect the mechanical properties and dimensional accuracy of the printed parts.

2.1. Powder characterization

Powder X-ray diffraction (XRD) characterization was carried out using PANalytical Empyrean (Serial No: DY1032, PANalytical, Netherlands) X-ray diffractometer with Cu–Kα radiation. JCPDS files were used to identify the main components in samples.

The particle size and particle size distribution of 3DP Zp150 powders were determined using a particle size analyzer (Mastersizer MV, Malvern Instruments Ltd, UK). The powder materials were scanned three times to find out the D_{10}, D_{50}, and D_{90} values which are the diameters were 10%, 50%, and 90% of the particles lie below those sizes, respectively.

2.2. Design of scaffolds

In this study, a scaffold was considered as a cylindrical structure shaped by an extruding cut by small cubicle elements named unit cell. The height and the diameter of scaffolds circumscribed the number of unit cells in each class of scaffold.

Geometry of scaffold was chosen as it represents the typical

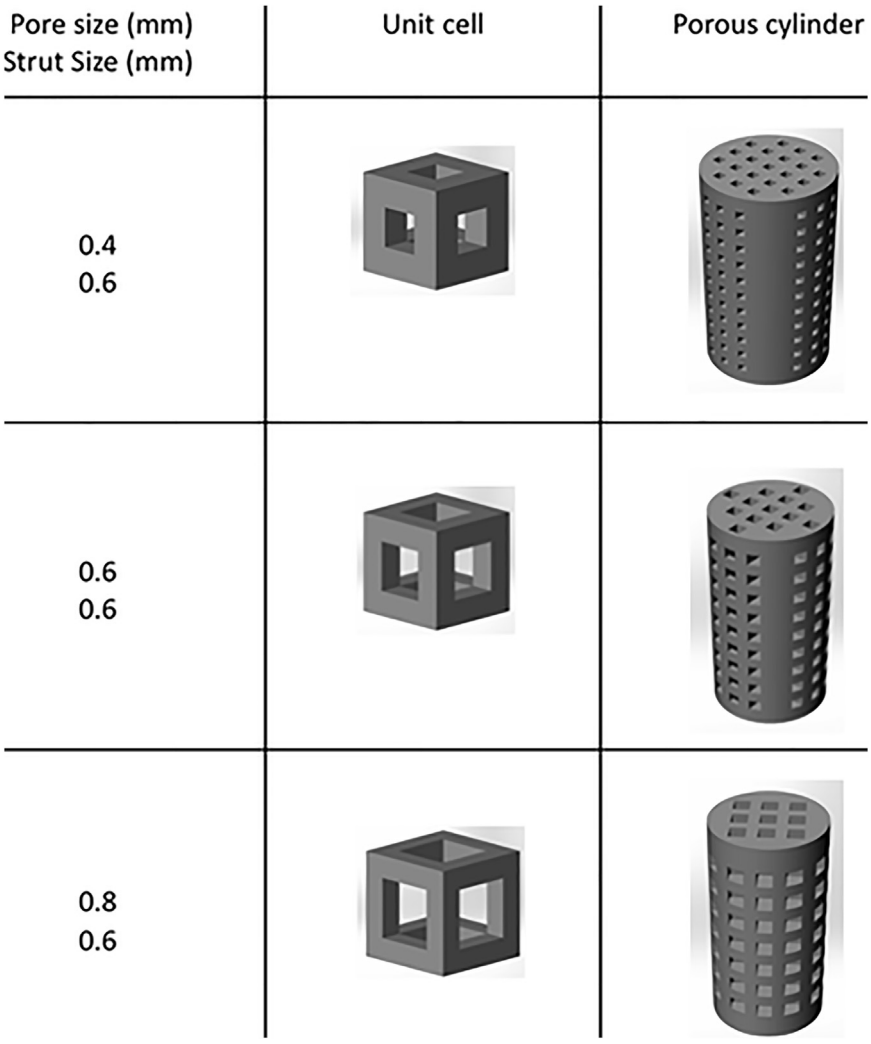

Fig. 1. CAD design of unit cells and porous scaffolds.

features and features sizes found in bone tissue engineering scaffolds intended to replace or repair an anatomical deficiency of *in vivo* tests [2]. However, the definition of an adequate pore size is still the matter of debate [1], it is generally reported to be in the range 100–800 μm [19].

Scaffold Prototype with 12 mm height, 6 mm diameter with three different pore sizes in unit cell were designed using the 3D design software, SolidWorks® 2012 and exported as STL file. Three different classes of porous scaffolds prototypes were designed and constructed, they are illustrated in Fig. 1 and their specification is listed in Table 1. The classes denominated as pore size for each unit cell.

Table 1
The specification of CAD design scaffolds.

Pore size (mm) Strut size (mm)	Porosity percentage (%)	Volume of porous cylinder[a] (mm^3)	Specific surface area (mm^2)
0.4 0.6	23.60%	80.09	948.81
0.6 0.6	36.34%	123.31	909.95
0.8 0.6	45.04%	152.84	812.21

[a] The volume of full cylinder (mm^3)=339.29.

In their review, Butscher et al. [20] mentioned that despite the massive potential of free-form fabrication methods for making samples with micro-pore size, practically only scaffolds with pores larger than 500 μm have been successfully fabricated to date.

2.3. Printer parameters

A plan of experiments, based on a full factorial design of experiments, was used to optimize the settings of process parameter values for improving quality characteristics of the scaffold prototypes. Optimal processing parameters were defined as those that yielded parts that most closely resembled an ideal 3DP part. An ideal 3D printed processed part was defined as one that (a) had sufficient green strength and easily de-powdered (b) was dimensionally accurate, (c) possessed interconnected pores and (d) proper porosity. The 3DP process parameters examined in this study were layer thickness, the delay time in spreading a new layer, and build orientation. Table 2 shows the design of experiment factors and their levels investigated in this study.

2.3.1. Layer thickness

In 3DP processes, the layer thickness refers to the height of the powder bed that is spread along the *z*-axis during the procedure. Previous studies developed by [20], [17] and [21] showed the layer thickness has significant effects on scaffold physical properties.

Table 2
The design of experiment's factors and their levels.

No.	Parameter	Unit	Level 1	Level 2	Level 3	Level 4
1	Layer thickness	μm	88.90 ≈ 89	101.60 ≈ 102	114.30 ≈ 114	127.00
2	Delay time	Second	0.05	0.10	0.30	0.50
3	Build orientation	–		*y*	*z*	–

2.3.2. Build orientation

Among the various process parameters, part orientation seems to have the greatest impact [11]. Therefore, it was rational to consider the interaction of other parameters with respect to orientation. Consequently, the orientation was selected as one of the main factors. A specimen's arrangement on the build bed and the number of each sample group is shown in Fig. 2. Because of the location of binder and its movement, which is from left to right, samples were located in three groups for each orientation; eight samples were used for each group to remove the influence of specimen location.

2.3.3. Delaying the spreading of the new layer (delay time)

The Zprinter® 450 software has a default delay of 100 ms between the ends of spreading one layer to the start of spreading the next. We refer to this delay as the *delay time*. We decided to assess whether increasing the powder delay time (300 or 500 ms) would allow further binder relaxation and densification, particularly in pores and channels, as each layer would have additional exposure time. However, we also hypothesized that the added time could impact layer-to-layer bonding, which would consequently affect the mechanical behavior of specimens as well as their dimensions. Therefore, a shorter time delay, 50 ms, was also selected to evaluate this theory.

2.4. Design matrix and experimental procedures

A full factorial design of experiments (DOE) was used to determine optimal 3DP parameters of scaffold prototype processing. Optimal processing parameters were defined as those that resulted in parts as perfectly processed parts as possible. The multiple performance measures considered herein were the percentage changes in diameters and height of built parts, porosity, and compressive strength.

Signal to noise (S/N) ratio and analysis of variance (ANOVA) were employed to study the important factors which significantly influenced dimensional accuracy and mechanical properties. ANOVA was performed to see whether the factors were statistically

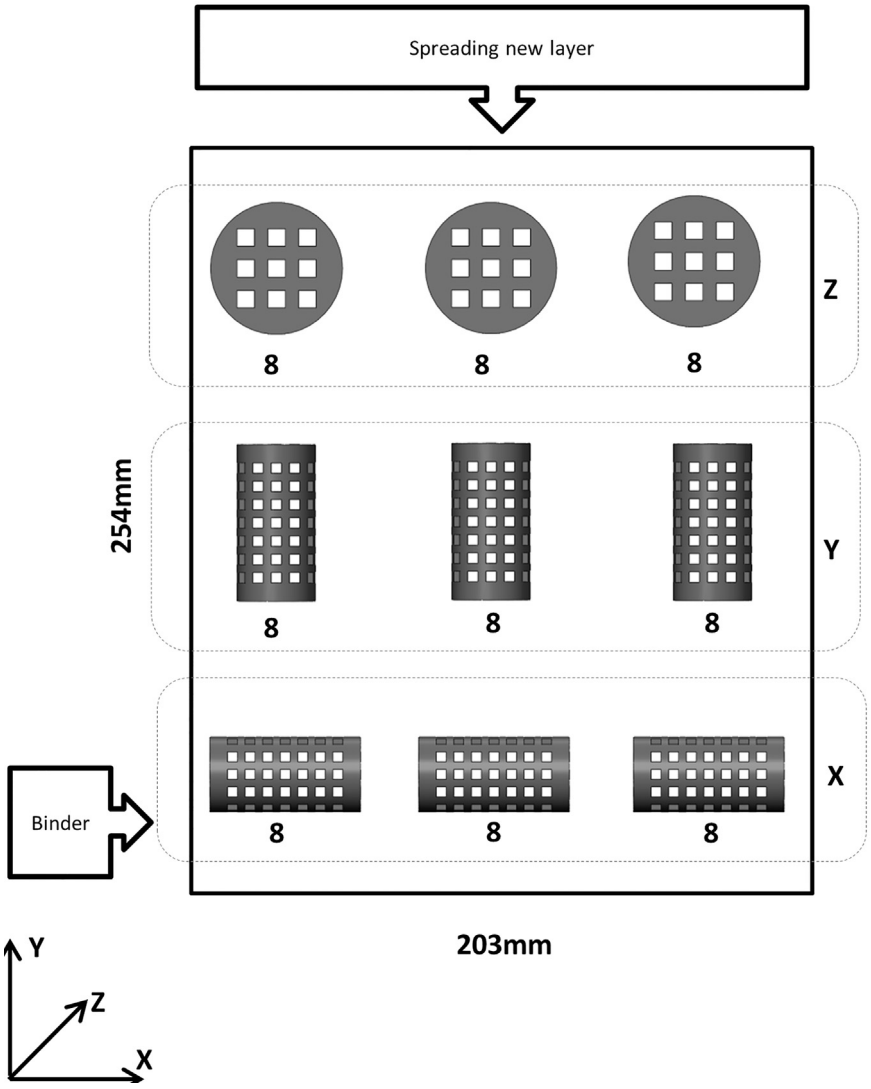

Fig. 2. Top view of Zp450 Build bed Size and specimens arrange and number for each run set.

significant or not *via* the sum of squares, *F*-value, and *P*-value. *P*-value is the probability value used to identify whether an effect in the model was statistically significant [22]. The smaller the value of *P*, the more significant is the corresponding coefficient. In the present work, a *P*-value should have been less than or equal to 0.05 or 0.01 (95% and 99% confidence levels, respectively) for the effect to be statistically significant. A commercial statistical package, Design-Expert version 7, was utilized for the design of experiments.

2.5. 3D printed parts characterization

3D printed part quality was defined by three characteristic features: (1) mechanical properties (2) dimensional accuracy, and (3) porosity. We used these features to evaluate the quality of the printed scaffolds for all DOE test samples. The importance of the selected parameters and the methods used for measurements are described in detail in the following section.

2.5.1. Mechanical properties

Green strength refers to the initial strength after printing and before any post-processing to increase mechanical properties. In this study, no post-processing techniques were employed to evaluate the feasibility of 3D machine parameters to build porous scaffolds. Clearly, green strength is a key property of a printed scaffold and describes the mechanical characteristics immediately after extraction from the powder bed and after de-powdering (removing unbound powder) [23]. Insufficient green strength may result in shape changes or eventually mechanical failure of the green body. Even the weight of the unbound powder might be critical for a weak scaffold structure. The green strength of the printed part depends on mainly two factors: the strength of the bonds between adjacent particles and the bond strength between neighboring layers. An optimal green strength is required to meet the mechanical property demands of scaffolds because the green strength will affect the final strength (after any post processing, *e.g.*, sintering or dipping into a binder solution) [24].

Uniaxial compressive testing was conducted using a mechanical testing instrument with 10 kN load-cell (Instron 5848 Micro Tester, USA) and a cross-head loading rate of 0.5 mm min^{-1}. Nine cylinders of each type (6 mm in diameter and 12 mm in height) were made for tests. We reported the maximum stress recorded as the compressive strength, and we considered the slope of linear region before the yield point as the Young's modulus.

2.5.2. Dimensional accuracy

Dimensions (the diameters and height of two sides of the fabricated specimens) for each of the 24 test parts for 48 runs were measured using a Mitutoyo digital caliper having a least count of 0.01 mm. The readings were then recorded, averaged and compared with their target dimension by calculating the deviation as a percent difference.

We defined a dimensional distortion ratio (DDR), and used those criteria to quantify the distortion or asymmetry of printed parts. The DDR can be calculated simply using Eq. (1).

$$\mathrm{DDR} = \frac{d_{CAD}}{h_{CAD}} - \frac{d}{h} \tag{1}$$

Where d and h are the averaged measured value of diameters and height, d_{CAD} and h_{CAD} are the computer aided design (CAD) model diameter and height, respectively. When there is no distortion, the DDR is equal to zero. Non-zero numbers mean height or diameter distortion: negative if the height is more than the diameter and positive if the diameter is more that the height.

Isotropy is a measure of the three dimensional asymmetry or the existence or lack of preferential alignment along the specific structural directions. Apart from the percent volume, degree of anisotropy (DA) and the general stereology parameters of bone are probably the most important determinants of mechanical strength.

Here, a DA of 0 corresponds to fully isotropic samples and tends to 1 as samples become increasingly anisotropic (a DA of 1 represents full anisotropy). The DA values were reported by the CT-analyzer software.

In this study, the measurement of height and diameter, DDR and DA were the three factors considered for evaluation of the dimensional accuracy.

Scanning electron microscopy (SEM) was employed (Quanta FGG 250, Holland) to capture pictures for calculation of the average pore size and strut size and to study the microstructure of the printed scaffolds. Close up images of specimens were taken by a digital camera (Canon G12, Japan).

2.5.3. Porosity

Cell seeding efficiency, diffusion properties, and mechanical strength of a scaffold are directly influenced by porosity. a successful scaffold must meet several requirements; the one of foremost importance is the existence of interconnecting channels to enable the supply of nutrients and metabolites to allow cell ingrowth [9,25]. In this context, the analysis of the scaffold porosities is of great relevance. Numerous methods which can be used to analyze pores are optical approaches (microscopy), physicochemical approaches (nitrogen adsorption and desorption), and capillary approaches (mercury porosimetry) [25]. However, only advanced medical imaging techniques such as micro-computed tomography (micro-CT) and magnetic resonance imaging (MRI) can provide a 3D image of the scaffold.

3D imaging is a nondestructive method which allows close up inspection of a specific location. We can observe the pore shape and measure the pore size and strut/wall thickness, porosity and pore interconnectivity by using the 3D images [26,27]. One test specimen from each test (Table 4) was scanned using a micro-CT (SkyScan *in-vivo* XRay 1076, Belgium).

The scanner used in the experiments was a high resolution, compact desktop unit. For each specimen, nearly 700 scan slices were taken. When analyzing the porosity of the scaffolds, the threshold to be used was readily obtained for each individual specimen by the threshold histogram offered by the SkyScan software.

3. Result and discussion

3.1. Powder and binder characterization and scaffold fabrication

Plaster-based powder has the advantage of setting fast with good strength, low cost and harmless to humans making it suitable for model making. Plaster of Paris (Bassanite) or calcium hemihydrate ($CaSO_4 \cdot 1/2H_2O$) was among the first materials used for 3D printers. It can be wetted by commercially formulated binder; subsequently, by activating the self-hydration process, a gypsum paste ($CaSO_4 \cdot 1/2H_2O + 1\ 1/2H_2O = CaSO_4 \cdot 2H_2O$) forms, as shown by Butscher, Bohner, Hofmann, Gauckler and Müller [20]. This material was supplied by Z-corporation in powder form (Zp150) and was used without further treatment.

The binder used in this work (Zb63) was a clear, 98% water content, commercially formulated 2-pyrrolidone solution. It was an aqueous solution, very similar to water, and according to the safety sheet is not classified as a hazardous substance. The pH of the binder at 20 °C was 9.8, its boiling point was 100 °C and it had a density of 1 g/cm3. The viscosity of the binder was almost similar

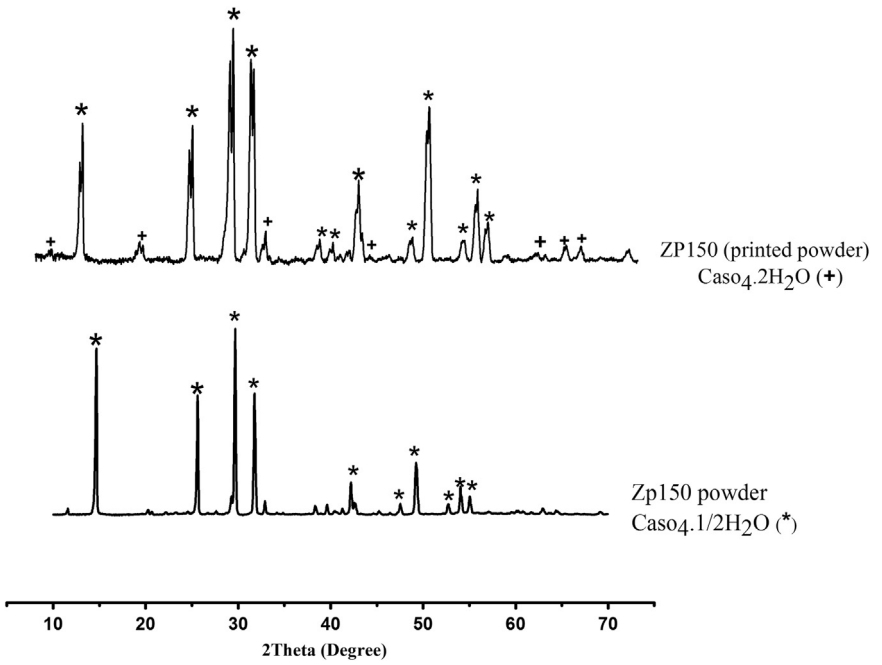

Fig. 3. XRD pattern of ZP150 powder (before and after printing).

to that of water.

The XRD spectra obtained for the Zp150 powder before and after sample fabrication. The results of the X-ray diffraction phase analysis are given in Fig. 3. According to ICDD card No. 24-1067 and 6-0046 the pattern demonstrated that the ZP150 consisted of calcium hemihydrate ($CaSO4 \cdot 1/2H_2O$) and gypsum paste ($CaSO_4 \cdot 2H_2O$) phases before and after printing, respectively. CaSO4 is a biocompatible and biodegradable material and its implants have shown the capability to provide a framework for attachment of osteoblast cells. It also can easily be reabsorbed by osteoclasts. One of the major disadvantages of $CaSO_4$ is its low mechanical strength and fast degradation rate [28]. Previous studies showed that post-processing techniques or composition with other biocompatible materials could improve the properties of $CaSO_4$-based materials for bone scaffold applications [29,30].

In the present work, we mainly studied the influence of printing parameters on manufacturing of the porous structures and physical properties of 3D printed prototypes. In the stage of the research, when we have the structurally and mechanically optimized samples, next we need to conduct some cytotoxicity, *in vitro* and even *in vivo* tests to get a better insight of the biological behavior of the printed scaffolds.

A previous study by Utela, Storti, Anderson and Ganter [31] shows that for the 3DP process the most important powder property is deposit-ability, which depends on the size and shape of the particles. The powder can be deposited in a dry or wet state, albeit, the proper particle size is different for each state. In a dry state, particles larger than 20 μm are preferentially deposited, but particles smaller than 5 μm can be deposited in either the dry or wet state.

The commercial ZP150 powder had a particle size distribution as $D_{10}=0.64$, $D_{50}=27.36$, and $D_{90}=68.83$ μm indicates that 10%, 50%, and 90% of the particles lie below those sizes, respectively, which were suitable for 3DP process on the machine used in this work.

Scaffolds were fabricated using 3DP for each of the design series (pore sizes of 0.4, 0.6, and 0.8 mm). After build-up, all of the scaffolds possessed sufficient green strength to withstand the air gun pressure during removal of the unbound powders (de-powdering process). However, it was difficult to remove all of the unbound powder from the scaffolds with a pore size of 0.4 and 0.6 mm. Therefore, we chose the minimum feature size of 0.8 mm.

The results obtained suggested the minimum pore size required for an acceptable definition, for the geometries studied, is 0.8 mm, which has is smaller than results of [18] and [32], who found the minimum sizes to 1 mm and 1.2 mm pore size, respectively. Fig. 4 shows the details of a fabricated specimen with pore sizes of 0.4 and 0.6 and 0.8 mm, which illustrated a lack of parallelism between the faces, and indicated poor geometric control of macro-pores of samples with a pore size of 0.4 and 0.6 mm (Fig. 4a and b) compared to a pore size of 0.8 mm (Fig. 4c and d). Moreover, the SEM images and micro-CT analysis showed that specimens with a pore size of 0.8 mm had an interconnected pore structure indicating that the unbound powder was totally removed in the de-powdering step (Figs. 5 and 6).

3.2. Dimensional features

In preliminary tests, it was noted that the size of printed parts did not accurately match the CAD design. The deviations were between 0.01 and 0.60 mm for both the diameter and the height. The average measurement of all samples is summarized in Table 3.

The results of SEM images and micro-CT analysis showed the macro-pore size of all specimens was less than the CAD design. This can be explained by the unbound powders that were not totally removed during the de-powdering process. The macro-pore size of all specimens was approximately between 680 μm and 750 μm. The specimens fabricated in the *x*-direction in all test conditions were de-powdered completely and rapidly compared to other specimens fabricated in other directions. The circular cross section of *z*-direction fabricated samples and cylinder wall of the *y* and *x* directions fabricated sample required more time to de-powder. This finding could be related to the fact that these sections were the first fabricated layers in the printing procedure for each specimen and due to the amount of binder relative to the powder without any previous printed structure; thus, the powder piled upon itself making the de-powdering step more difficult.

As a result, the percentage of change in the macro-pore size

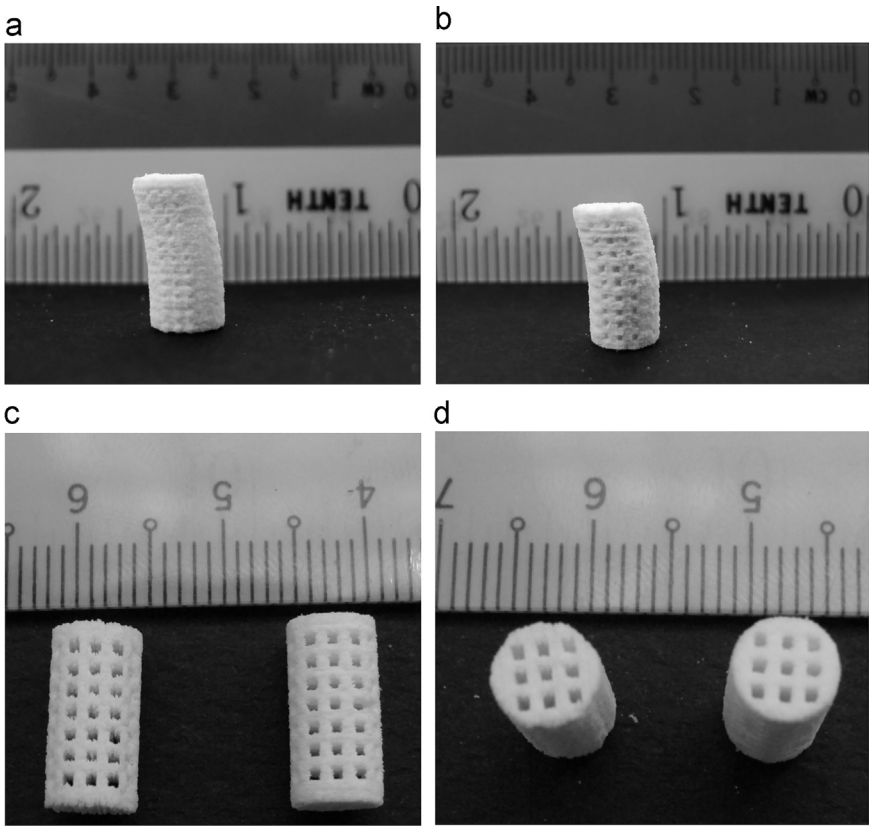

Fig. 4. Fabricated scaffold using the (a) unit cell type 1-Pore size: 0.4 mm- (b) unit cell type 2-Pore size: 0.6 mm (c) side view (d) top view of the Unit cell type 3-Pore size: 0.8 mm.

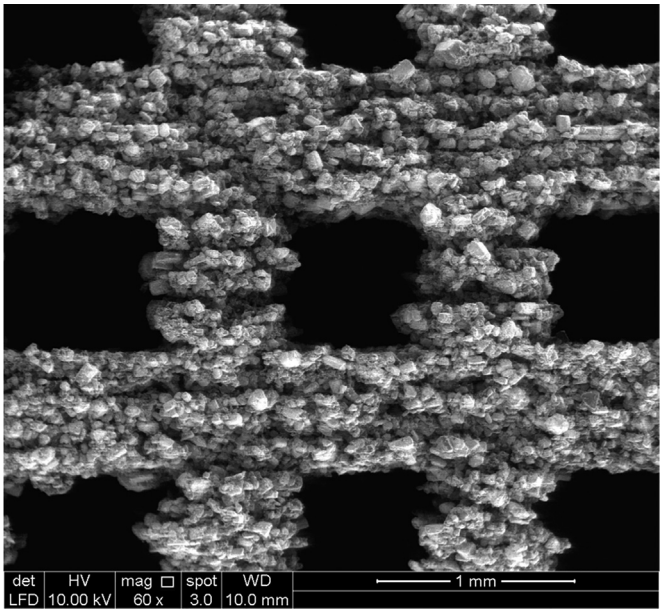

Fig. 5. SEM images- fabricated scaffold using Unit cell type 3-Pore size: 0.8 mm.

was between 6% and 15% compared with the CAD design. The strut size of all specimens was between 600 and 610 μm, which is in close agreement with the CAD design size. It is well accepted that for bone tissue engineering purposes, the macro-pore size should be in the range of 200–900 μm [7,8,33]. Accordingly, it seems that the macro-pores we achieved in this research indicate scaffolds appropriate for bone tissue engineering applications.

The diameter of all specimens was less than the diameter of CAD model (6 mm). The height of the scaffolds, except the specimens fabricated in the *z*-direction, are also less than that of the design.

Fig. 7 shows the dimensional deviation ratio of all fabricated specimens. Most of the samples exhibited height deviations during the fabrication. Moreover, samples built in the *z*-direction in each layer thickness and delay time had more height changes in contrast with other orientations. Samples fabricated in the *x*-direction for all delay times and layer thicknesses had the least changes in height. Samples printed in the *x*-direction and with a delay of 300 ms in each of four layer thicknesses had the least distortion.

The ANOVA and model *F*-value of DDR (3.66) imply the model is statistically significant. There is only a 0.28% chance that these values occur due to noise.

The *P*-value of orientation (< 0.0001) shows that the changes in the orientation value relative to changes in the response variable were significant. For dimensional deviation, the ratio orientation with a 36.62% contribution was the most significant model term. The standard deviation of the model was 0.027. The model signal-to-noise ratio (7.33) indicated an adequate signal because a ratio greater than four was desirable.

DA plays an important role in dimensional accuracy. In this work, DA=0 represents complete isotropy, while DA=1 represents complete anisotropy. Because the CAD design was symmetrical, a printed scaffold with a lower DA would possess a greater dimensional accuracy than a sample with a larger DA. The DA values of all 48 samples fabricated scaffolds are listed in Table 4. As evident, the samples printed in the *x*-direction in all layer thicknesses and all delay times were more isotropic in comparison than those printed in either the *z* or *y* direction.

Due to the greater degree of isotropy, samples fabricated in the *x*-direction were also selected for further investigation. The specimens that were fabricated with a 300 ms delay time had lower

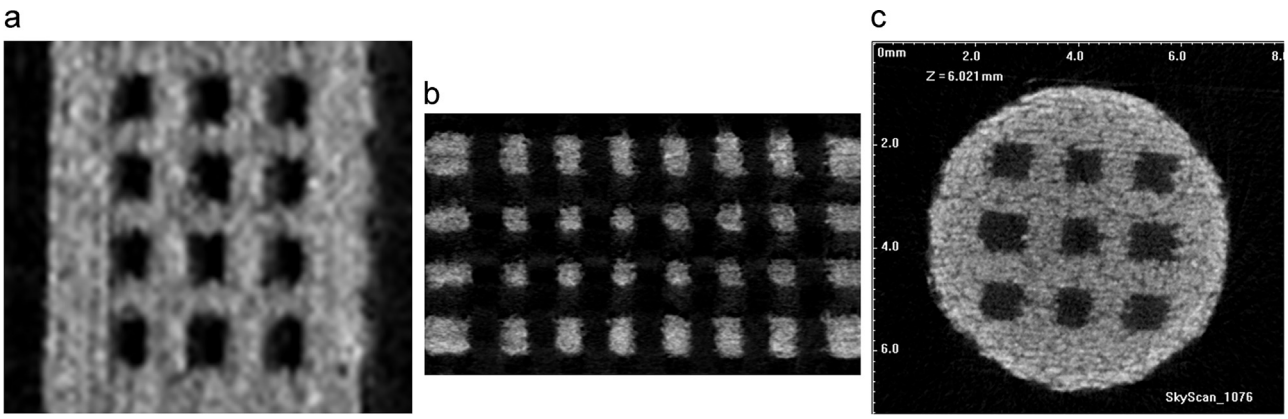

Fig. 6. Micro-CT images-fabricated scaffold using Unit cell type 3-Pore size: 0.8 mm (a) front view, (b) middle cross-section view (C) top view.

DA values than the other samples. Moreover, specimens fabricated with thinner layer thicknesses, and with a delay of 300 ms, were the most isotropic. The prototypes printed with a layer thickness of 89 μm and a delay time of 300 ms were the most isotopic samples

The *F*-value of the degree of anisotropy (11.60) indicates the model is significant. "Prob > *F*" value of orientation suggested that orientation was the most significant term in the model with a 37% contribution, while layer thickness delay was also significant but to a lesser degree. The model signal-to-noise ratio was 12.980.

There were two main factors which directly had an effect on dimensional accuracy: (1) solidity of each layer and (2) compaction of sequential layers [20,34]. Previous studies indicated that powder and binder reactivity can play a considerable role in 3DP procedures. Additionally, adequate timing significantly affects the reactivity of the powder and binder as well as their bonding [9,24].

Both the DDR and DA results suggested that an increase in the delay time resulted in better bonding between powder and binder and produced 3D objects with an improved dimensional accuracy and isotropy. However, there is a trade-off between choosing time for better bonding of powder intra-layer and inter-layer. A greater delay time might cause complete binder dryness which is desirable for reactivity of binder and powder within a layer but reduces the bonding capability of the powder to next layer resulting in discrete layering rather than a homogenous part. This condition significantly influences the dimensional accuracy and mechanical features of the 3D printed parts.

Supporting these hypotheses, the results also showed that additional time exposure of a printed layer allowed further binder relaxation and had a positive effect on the structural features of a printed sample. In contrast, a delay time greater than 300 ms had a negative effect on the prototypes, due to poor bonding between neighboring printed layers.

In this study, by evaluating sample dimensions (diameter and height) as well as DDR and DA factors, it was found that the specimens fabricated in the *x*-direction using the minimum layer thickness and a 300 ms delay time yielded the greatest dimensional accuracy.

3.3. Mechanical features

The results of mechanical compression tests (Table 5) showed that differences in each process parameter resulted in various compressive strengths and Young's moduli. Specimens fabricated in the *x*-direction in each layer thickness and delay time had greater compressive strength than specimens built in either the *z* or *y* direction. Insufficient compressive strengths of *z*-direction fabricated led to fracture for some samples during de-powering. For all layer thickness and build orientations, the specimens fabricated with a 300 ms delay time had greater compressive strengths than others.

The results showed that the orientation of the powder spreading and binder jetting affected the mechanical behavior of the printed parts. In the *x*-direction fabricated samples, the compressive load was applied parallel to the direction of printed layers and perpendicular to the direction of the binder jetting. In contrast, in the *y*-direction printed samples compressive loads were applied parallel to the direction of printed layers and perpendicular to the direction of binder jetting. Moreover, a decrease in layer thickness causes an increase in the number of layers.

Fig. 8 shows the schematic view of binder droplets that jetted in each direction. In the specimens printed in *Z* and *Y* directions, the binder jetted on the circular cross sections. In contrast, in the specimens printed in the *X* direction, the binder jetted along the height of the samples. When the next powder layer spread, it was bonded to the previous layer in the binder-jetted area. In the X-printed samples, the area that each layer bound with next and previous layers were in the direction of the height of the scaffold whereas in the samples printed in the *Y* and *Z* directions were in the direction of the diameter. In the Z-printed samples the layers

Table 3
The measurement of diameter and height of the 3D printed porous scaffolds.

Layer thickness (μm)			89				102				114				127			
			50	100	300	500	50	100	300	500	50	100	300	500	50	100	300	500
Diameter (mm)	Orientation	X	5.84	5.99	5.84	5.88	5.79	5.96	5.78	6.04	5.78	5.82	5.85	5.85	5.87	5.89	5.85	5.86
		Y	5.80	5.93	5.78	5.83	5.77	5.94	5.71	5.85	5.82	5.90	5.79	5.82	5.85	5.88	5.82	5.83
		Z	5.79	5.82	5.79	5.82	5.78	5.82	5.77	5.76	5.79	5.77	5.78	5.76	5.84	5.81	5.80	5.89
Height (mm)		X	11.76	11.77	11.73	11.76	11.74	11.76	11.68	11.76	11.81	11.76	11.78	11.75	11.78	11.78	11.77	11.83
		Y	11.78	11.81	11.78	11.42	11.78	11.82	11.80	11.82	11.82	11.86	11.85	11.82	11.83	11.85	11.83	11.90
		Z	12.05	12.31	12.08	12.14	12.01	12.14	11.90	12.36	11.97	12.17	12.01	12.02	12.09	12.23	11.87	11.89

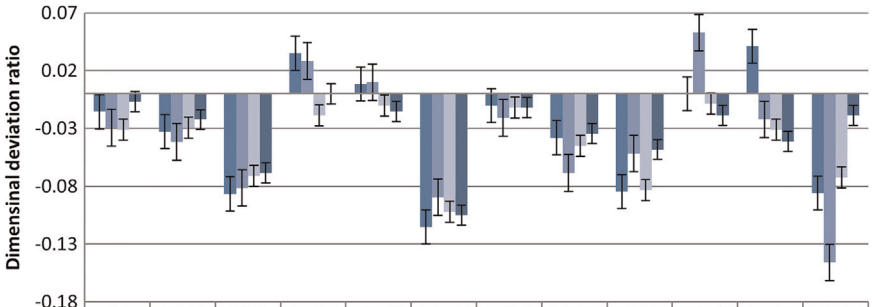

	50-X	50-Y	50-Z	100-X	100-Y	100-Z	300-X	300-Y	300-Z	500-X	500-Y	500-Z
102	-0.02	-0.03	-0.09	0.04	0.01	-0.12	-0.01	-0.04	-0.08	0.00	0.04	-0.09
114	-0.03	-0.04	-0.08	0.03	0.01	-0.09	-0.02	-0.07	-0.05	0.05	-0.02	-0.15
127	-0.03	-0.03	-0.07	-0.02	-0.01	-0.10	-0.01	-0.04	-0.08	-0.01	-0.03	-0.07
89	-0.01	-0.02	-0.07	0.00	-0.02	-0.10	-0.01	-0.03	-0.05	-0.02	-0.04	-0.02

Fig. 7. Dimensional accuracy ratio of all 48 runs for each layer thickness, delay and orientation.

Table 4
Degree of anisotropy of all 48 runs for each layer thickness, delay time and orientation.

Layer thickness (μm)			89				102				114				127			
Delay* (ms)			50	100	300	500	50	100	300	500	50	100	300	500	50	100	300	500
Degree of anisotropy	Orientation	X	0.64	0.59	0.43	0.49	0.51	0.63	0.45	0.49	0.55	0.55	0.54	0.59	0.51	0.62	0.47	0.47
		Y	0.71	0.66	0.62	0.62	0.64	0.60	0.59	0.60	0.66	0.68	0.67	0.69	0.72	0.71	0.56	0.67
		Z	0.77	0.74	0.68	0.78	0.70	0.70	0.70	0.80	0.77	0.77	0.77	0.77	0.77	0.77	0.69	0.73

Table 5
Mechanical property assessment of porous 3D printed specimens.

Layer thickness (μm)			89				102				114				127			
Delay (ms)			50	100	300	500	50	100	300	500	50	100	300	500	50	100	300	500
Compressive strength (Mpa)	Orientation	X	0.44	0.37	0.75	0.62	0.56	0.34	0.58	0.48	0.40	0.47	0.76	0.65	0.46	0.50	0.56	0.50
		Y	0.25	0.27	0.42	0.26	0.34	0.20	0.31	0.27	0.17	0.37	0.39	0.30	0.24	0.43	0.44	0.28
		Z	0.18	0.23	0.37	0.21	0.25	0.22	0.30	0.22	0.19	0.32	0.33	0.25	0.19	0.25	0.30	0.25
Young's Modulus		X	27.70	19.65	47.15	26.26	36.27	17.96	34.47	23.16	23.71	29.22	46.08	25.12	27.10	21.56	26.67	24.77
		Y	11.80	10.36	18.27	11.89	16.60	7.41	12.29	9.13	12.01	17.05	19.56	16.03	10.42	17.13	17.52	9.24
		Z	4.21	4.28	7.72	3.84	4.98	3.95	4.61	2.09	2.27	7.06	5.64	3.05	2.79	4.01	5.08	2.83

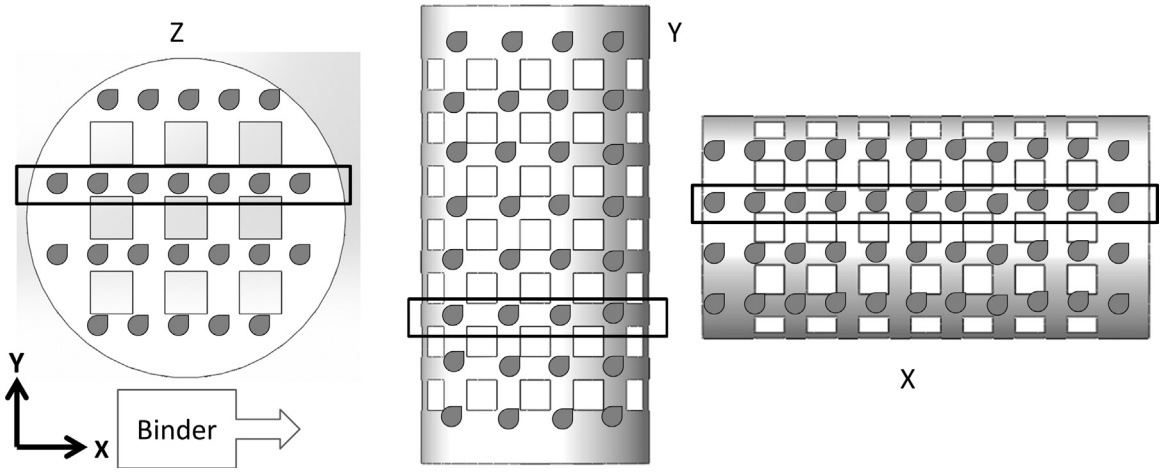

Fig. 8. The binder jetting in printed samples.

were bonded to each other in the circular cross section which resulted in a lower mechanical strength. This is due to a smaller contact area of successive layers than the *X* and *Y* directions. Nevertheless, in the *X* direction the successive layers were bonded to each other in the larger area along the cylindrical cross section. This resulted in higher integrity of the layers that in turn increased

Table 6
Porosity of 3D printed specimens.

Layer thickness (μm)			89				102				114				127			
Delay (ms)			50	100	300	500	50	100	300	500	50	100	300	500	50	100	300	500
Closed porosity	Orientation	X	0.83	0.25	0.29	0.20	0.17	0.05	0.90	0.14	0.02	0.46	0.73	0.61	0.22	0.91	0.10	0.24
		Y	0.81	0.01	0.08	0.18	0.19	0.05	0.88	0.08	0.02	0.76	0.50	0.60	0.83	0.87	0.11	0.10
		Z	0.79	0.01	0.06	0.90	0.27	0.02	0.08	0.77	0.46	0.73	0.59	0.89	0.98	1.28	0.08	0.09
Open porosity		X	65.17	45.18	67.62	61.56	61.37	40.91	63.01	57.29	38.25	72.07	63.33	63.70	62.82	63.31	60.85	59.33
		Y	66.00	43.06	62.61	61.62	64.50	43.34	60.86	55.45	35.28	67.94	65.16	65.79	65.62	63.31	63.32	61.27
		Z	64.78	42.54	61.93	63.40	71.49	42.78	60.88	61.72	61.21	66.75	66.65	65.87	65.17	62.37	60.79	55.93
Total Porosity		X	65.46	45.32	67.71	61.64	61.43	40.93	63.34	57.35	38.26	72.20	63.60	63.92	62.90	63.65	60.89	59.43
		Y	66.28	43.07	62.64	61.70	64.57	43.36	61.20	55.48	35.29	68.18	65.34	65.99	65.90	63.63	63.36	61.31
		Z	65.06	42.55	61.95	63.73	71.56	43.93	60.91	62.01	61.39	66.99	66.85	66.17	65.51	62.86	60.82	55.97

Table 7
The optimum fabricated scaffolds in terms of compressive strength.

Layer thickness (μm)	Delay time (ms)	Degree of anisotropy	Compressive strength (Mpa)	Young's modulus	Close porosity	Open porosity	Total porosity (%)
89	300	0.43	0.75	47.15	0.29	67.62	67.71
114	300	0.64	0.76	46.08	0.73	63.33	63.60

the strength of the specimens.

These results also indicated the interaction between the layer thickness and the delay time parameters had a considerable effect on the mechanical strength of printed samples. By focusing on *x*-direction fabricated specimens, which have the greatest compressive strengths, we conclude that the specimens fabricated by thinner layer thicknesses and lower delay times possessed lower mechanical integrity due to poor bonding between powder particles in each layer and also the densification of neighboring layers.

The model *F*-value of 17.58 for the mechanical features implied the statistical model was significant at the selected confidence level. In this case, significant model terms were delay, orientation, interaction between layer thickness and delay time. Among these, orientation with a nearly 34% contribution, is the most significant term. The model signal-to-noise ratio (16.612) showed an acceptable signal.

3.4. Porosity

The results for porosity (Table 6) showed that specimens built in the *x*-direction are more porous than samples were printed in the *z* or *y* direction. Specimens printed in the *x*-direction with a 114 μm layer thickness and 100 ms delay time had the maximum porosity. In our previous work [35] that we studied the different layer thicknesses with the machine default delay (100 ms), the samples printed in *X* direction with 114 μm layer thickness had more porosity than the other samples. The present study revealed that the different delay times did not improve the porosity of printed samples compared with our previous work.

According to [25] there is a general agreement that 3D bone scaffolds should have a highly open porous structure ($>$ 40–60%). Moreover, in bone tissue engineering the key factor in bone regeneration is the ability of scaffolds to conduct fluid flow. This parameter, called permeability, directly depends on porosity and interconnectivity of the printed samples [36,37].

The model *F*-value was 8.79. Layer thickness, delay time, and two-way interaction between the delay time and layer thickness played an important role in porosity and significant model terms, among which, the interaction between the delay time and layer thickness with an 8% contribution is the most significant factor in porosity. The model signal to ratio (10.901) indicated an adequate signal.

Table 7 summarizes the results of two specimens printed in the *X* direction and had highest compressive strength. Despite the fact that these two samples approximately had the same compressive strength, the samples printed with an 89 μm layer thickness and a 300 ms delay time were more isotropic and porous with better pore spacing and openness. These samples also had greater Young's moduli. Thus, the optimal 3DP processing conditions were *x*-direction orientation with a minimum layer thickness and a 300 ms delay time for scaffold prototypes for bone tissue engineering applications.

These results compared with our previous study [35] show that by choosing the minimum layer thickness, an additional 200 ms is needed for consistent setting of powder and binder. This additional time allows better densification of adjacent powder particles and between sequential layers, which improves the mechanical strength of the printed specimens.

4. Conclusion

Cylindrical calcium sulfate-based porous scaffold prototypes were successfully designed with three different pore sizes and fabricated with different setting parameters using a commercial 3D printer. Three significant factors that affect the printing process of porous specimens, namely, layer thickness, the delay time of applying the new layer, and build orientation, were systematically investigated in this study based on a design of experiments approach.

We found that fabricated scaffold prototypes with pore sizes of 0.4 and 0.6 mm deviated significantly from the CAD design on the bases of parallelism, distortion, and unconnected, closed pores; only prototypes with a pore size of 0.8 mm were considered for the design of experimental investigation. A full factorial DOE was used to investigate process parameters. Optimal processing parameters are defined as those that resulted in parts best resembling the CAD model. The various measures for analyzing the part

quality were percentage changes in diameters and heights, porosity, and compressive strength. The S/N ratio and ANOVA were used to study the optimal 3DP parameters for processing prototypes.

The study outcomes show that the specimens fabricated in the *x*-direction with the minimum layer thickness (89 μm) and that a 300 ms delay time provided the highest quality scaffold prototypes. Samples made with these parameters are deemed proper for bone tissue engineering applications due to high compressive strength, sufficient porosity, and dimensional accuracy, which are the most important factors for consideration when designing a bone scaffold.

Moreover, this study demonstrated the most significant parameters that directly influence dimensional accuracy, compressive strength, and porosity are orientation and delay time. Furthermore, the setting time needed for binder and powder reaction depends on the size of the layer thickness and is another factor affecting a part's physical properties.

The objective of this work was to re-tune the control factors of an existing rapid prototyping process for the given machine. We achieved these goals without major changes in the already developed hardware and software architecture. The optimal printing parameters were developed for the material used in this study. If one were to use another material formulation, these optimal printing parameters might not be appropriate. Nevertheless, the findings from this work can serve as a guideline to adjust the printing parameters for fabrication of other materials for different applications and to improve the ultimate characteristics of printed scaffolds.

Acknowledgment

This study was supported by High Impact Research Grant UM. C/HIR/MOHE/ENG/10 D000010-16001 from the University of Malaya.

Appendix A. Supplementary material

Supplementary data associated with this article can be found in the online version at http://dx.doi.org/10.1016/j.rcim.2015.06.005.

References

[1] M. Bohner, Y. Loosli, G. Baroud, D. Lacroix, Commentary: deciphering the link between architecture and biological response of a bone graft substitute, Acta Biomater. 7 (2011) 478–484.
[2] D.W. Hutmacher, Scaffolds in tissue engineering bone and cartilage, Biomaterials 21 (2000) 2529–2543.
[3] M. Dias, P. Fernandes, J. Guedes, S. Hollister, Permeability analysis of scaffolds for bone tissue engineering, J. Biomech. 45 (2012) 938–944.
[4] K. Leong, C. Cheah, C. Chua, Solid freeform fabrication of three-dimensional scaffolds for engineering replacement tissues and organs, Biomaterials 24 (2003) 2363–2378.
[5] E. Sachlos, J. Czernuszka, Making tissue engineering scaffolds work. Review: the application of solid freeform fabrication technology to the production of tissue engineering scaffolds, Eur. Cell Mater. 5 (2003) 39–40.
[6] D.W. Hutmacher, M. Sittinger, M.V. Risbud, Scaffold-based tissue engineering: rationale for computer-aided design and solid free-form fabrication systems, Trends Biotechnol. 22 (2004) 354–362.
[7] S. Krishnan, A. Dawood, R. Richards, J. Henckel, A. Hart, A review of rapid prototyped surgical guides for patient-specific total knee replacement, J. Bone Joint Surg. Br. 94 (2012) 1457–1461.
[8] M. Lee, B.M. Wu, Recent advances in 3D printing of tissue engineering scaffolds, Methods Mol. Biol. 868 (2012) 257–267.
[9] S. Bose, S. Vahabzadeh, A. Bandyopadhyay, Bone tissue engineering using 3D printing, Mater. Today 16 (2013) 496–504.
[10] P. Patirupanusara, W. Suwanpreuk, T. Rubkumintara, J. Suwanprateeb, Effect of binder content on the material properties of polymethyl methacrylate fabricated by three dimensional printing technique, J. Mater. Process. Technol. 207 (2008) 40–45.
[11] M. Castilho, M. Dias, U. Gbureck, J. Groll, P. Fernandes, I. Pires, B. Gouveia, J. Rodrigues, E. Vorndran, Fabrication of computationally designed scaffolds by low temperature 3D printing, Biofabrication 5 (2013) 035012.
[12] M. Castilho, C. Moseke, A. Ewald, U. Gbureck, J. Groll, I. Pires, J. Teßmar, E. Vorndran, Direct 3D powder printing of biphasic calcium phosphate scaffolds for substitution of complex bone defects, Biofabrication 6 (2014) 015006.
[13] A. Butscher, M. Bohner, N. Doebelin, L. Galea, O. Loeffel, R. Müller, Moisture based three-dimensional printing of calcium phosphate structures for scaffold engineering, Acta Biomater. 9 (2012) 5369–5378.
[14] A. Butscher, M. Bohner, C. Roth, A. Ernstberger, R. Heuberger, N. Doebelin, P. Rudolf von Rohr, R. Müller, Printability of calcium phosphate powders for three-dimensional printing of tissue engineering scaffolds, Acta Biomater. 8 (2012) 373–385.
[15] J. Suwanprateeb, R. Sanngam, T. Panyathanmaporn, Influence of raw powder preparation routes on properties of hydroxyapatite fabricated by 3D printing technique, Mater. Sci. Eng.: C 30 (2010) 610–617.
[16] T.J. Hsu, W.H. Lai, Manufacturing parts optimization in the three-dimensional printing process by the Taguchi method, J. Chin. Inst. Eng. 33 (2010) 121–130.
[17] J. Suwanprateeb, F. Thammarakcharoen, K. Wasoontararat, W. Suvannapruk, Influence of printing parameters on the transformation efficiency of 3D-printed plaster of paris to hydroxyapatite and its properties, Rapid Prototyp. J. 18 (2012) 490–499.
[18] M. Castilho, I. Pires, B. Gouveia, J. Rodrigues, Structural evaluation of scaffolds prototypes produced by three-dimensional printing, Int. J. Adv. Manuf. Technol. 56 (2011) 561–569.
[19] C. Liu, Z. Xia, J. Czernuszka, Design and development of three-dimensional scaffolds for tissue engineering, Chem. Eng. Res. Design 85 (2007) 1051–1064.
[20] A. Butscher, M. Bohner, S. Hofmann, L. Gauckler, R. Müller, Structural and material approaches to bone tissue engineering in powder-based three-dimensional printing, Acta Biomater. 7 (2011) 907–920.
[21] M. Vaezi, C.K. Chua, Effects of layer thickness and binder saturation level parameters on 3D printing process, Int. J. Adv. Manuf. Technol. 53 (2011) 275–284.
[22] G.P. Quinn, M.J. Keough, Experimental Design and Data Analysis for Biologists, Cambridge University Press, Cambridge, United Kingdom, 2002.
[23] A. Butscher, M. Bohner, N. Doebelin, S. Hofmann, R. Müller, New depowdering-friendly designs for three-dimensional printing of calcium phosphate bone substitutes, Acta Biomater. 9 (2013) 9149–9158.
[24] R. Chumnanklang, T. Panyathanmaporn, K. Sitthiseripratip, J. Suwanprateeb, 3D printing of hydroxyapatite: effect of binder concentration in pre-coated particle on part strength, Mater. Sci. Eng.: C 27 (2007) 914–921.
[25] J. Will, R. Detsch, A. Boccaccini, Structural and biological characterization of scaffolds, in: A. Bandyopadhyay, S. Bose (Eds.), Characterization of Biomaterials Oxford: Academic Press, Academic Press, Oxford, 2013, pp. 299–310.
[26] S.T. Ho, D.W. Hutmacher, A comparison of micro CT with other techniques used in the characterization of scaffolds, Biomaterials 27 (2006) 1362–1376.
[27] G.H. van Lenthe, H. Hagenmüller, M. Bohner, S.J. Hollister, L. Meinel, R. Müller, Nondestructive micro-computed tomography for biological imaging and quantification of scaffold–bone interaction in vivo, Biomaterials 28 (2007) 2479–2490.
[28] M. Murariu, L. Bonnaud, P. Yoann, G. Fontaine, S. Bourbigot, P. Dubois, New trends in polylactide (PLA)-based materials:"Green" PLA–Calcium sulfate (nano) composites tailored with flame retardant properties, Polym. Degrad. Stab. 95 (2010) 374–381.
[29] Y.-F. Tsai, C.-C. Wu, F.-Y. Fan, H.-C. Cheng, Y.-C. Liaw, Y.-K. Huang, L.-H. Hsu, K.-C. Yang, Effects of the addition of vancomycin on the physical and handling properties of calcium sulfate bone cement, Process Biochem. 49 (2014) 2285–2291.
[30] C.-C. Chen, C.-W. Wang, N.-S. Hsueh, S.-J. Ding, Improvement of in vitro physicochemical properties and osteogenic activity of calcium sulfate cement for bone repair by dicalcium silicate, J. Alloy. Compd. 585 (2014) 25–31.
[31] B. Utela, D. Storti, R. Anderson, M. Ganter, A review of process development steps for new material systems in three dimensional printing (3DP), J. Manuf. Process. 10 (2008) 96–104.
[32] Z. Zhou, F. Buchanan, C. Mitchell, N. Dunne, Printability of calcium phosphate: calcium sulfate powders for the application of tissue engineered bone scaffolds using the 3D printing technique, Mater. Sci. Eng.: C 38 (2014) 1–10.
[33] P.N. Streubel, W.M. Ricci, A. Wong, M.J. Gardner, Mortality after distal femur fractures in elderly patients, Clin. Orthop. Relat. Res.® 469 (2011) 1188–1196.
[34] A. Khalyfa, S. Vogt, J. Weisser, G. Grimm, A. Rechtenbach, W. Meyer, M. Schnabelrauch, Development of a new calcium phosphate powder-binder system for the 3D printing of patient specific implants, J. Mater. Scie.: Mater. Med. 18 (2007) 909–916.
[35] A. Farzadi, M. Solati-Hashjin, M. Asadi-Eydivand, N.A.A. Osman, Effect of layer thickness and printing orientation on mechanical properties and dimensional accuracy of 3d printed porous samples for bone tissue engineering, PLoS One 9 (2014) e108252.
[36] A. Farzadi, V. Waran, M. Solati-Hashjin, Z.A.A. Rahman, M. Asadi, N.A. A. Osman, Effect of layer printing delay on mechanical properties and dimensional accuracy of 3D printed porous prototypes in bone tissue engineering, Ceram. Int. 41 (2015) 8320–8330.
[37] S. Eshraghi, S. Das, Micromechanical, finite-element modeling and experimental characterization of the compressive mechanical properties of polycaprolactone–hydroxyapatite composite scaffolds prepared by selective laser sintering for bone tissue engineering, Acta Biomater. 8 (2012) 3138–3143.